Journal of Materials Chemistry A

PAPER

View Article Online
View Journal | View Issue

CrossMark click for updates

Cite this: J. Mater. Chem. A, 2014, 2, 18988

Effects of side chain isomerism on the physical and photovoltaic properties of indacenodithieno[3,2-*b*]thiophene–quinoxaline copolymers: toward a side chain design for enhanced photovoltaic performance

Xiaofeng Xu,[a] Zhaojun Li,[a] Olof Bäcke,[c] Kim Bini,[a] David I. James,[a] Eva Olsson,[c] Mats R. Andersson*[ab] and Ergang Wang*[a]

Four new D–A polymers PIDTT-Q-*p*, PIDTT-Q-*m*, PIDTT-QF-*p* and PIDTT-QF-*m*, using indacenodithieno[3,2-*b*]thiophene (IDTT) as an electron-rich unit and quinoxaline (Q) as an electron-deficient unit, were synthesized *via* a Pd-catalyzed Stille polymerization. The side chains on the pendant phenyl rings of IDTT were varied from the *para*- to the *meta*-position, and the effect of the inclusion of fluorine on the quinoxaline unit was simultaneously investigated. The influence on the optical and electrochemical properties, film topography and photovoltaic properties of the four copolymers were thoroughly examined *via* a range of techniques. The inductively electron-withdrawing properties of the fluorine atoms result in a decrease of the highest occupied molecular orbital (HOMO) energy levels. The effect of *meta*-substitution on the PIDTT-Q-*m* polymer leads to good solubility and in turn higher molecular weight. More importantly, it exhibits optimal morphological properties in the PIDTT-Q-*m*/$PC_{71}BM$ blends. As a result, the corresponding solar cells (ITO/PEDOT:PSS/polymer:$PC_{71}BM$/LiF/Al) attain the best power conversion efficiency (PCE) of 6.8%. The structure–property correlations demonstrate that the *meta*-alkyl-phenyl substituted IDTT unit is a promising building block for efficient organic photovoltaic materials. This result also extends our strategy with regards to side chain isomerism of IDTT-based copolymers for enhanced photovoltaic performance.

Received 8th August 2014
Accepted 30th September 2014

DOI: 10.1039/c4ta04102j

www.rsc.org/MaterialsA

Open Access Article. Published on 30 September 2014. Downloaded on 8/1/2025 7:07:04 PM.
This article is licensed under a Creative Commons Attribution 3.0 Unported Licence.

Introduction

As a novel solar energy harvesting medium, polymer solar cells (PSCs) have been intensively investigated in recent years as they offer the potential to be light weight, flexible and manufactured on a large-area scale at low cost.[1–4] So far, bulk-heterojunction polymer solar cells (BHJ PSCs), using a solution-processed active layer composed of an electron-donor and an electron-acceptor, sandwiched between ITO and metallic electrodes, can attain promising power conversion efficiencies (PCEs) of 8–9%.[5] Conjugated donor–acceptor polymers, combining an electron-donating (D) and an electron-withdrawing (A) moiety, are particularly promising now, since judicious selection of D and A moieties can tailor the D–A interaction and π-electron delocalization, to achieve tunable band gaps, energy levels and charge transporting properties for ideal electron-donor materials.[6–8] In principle, an effective strategy is to combine a weak D and a strong A unit alternately. The weak D moiety can anchor a low-lying HOMO level, whilst, the strong A moiety can provide a favorable LUMO level and a suitable band gap.[9] In addition, further optimization of a given D–A framework *via* improvements in solubility, molecular weight and structural orientation can be achieved through side chain modulation.[10–14]

To date, a variety of electron-rich arenes comprising of multiply fused aromatic systems have been reported.[15] Rigid backbones with horizontally or vertically extended π-conjugation can be formed by fastening or fusing adjacent building blocks to aromatic cores. One appealing electron-donating unit is the ladder-type indacenodithiophene (IDT) unit.[16–21] This structure of aromatic rings has enforced planarization which can easily suppress interannular rotation and enhance π-electron delocalization. The high degree of planarity is conducive to intermolecular charge-carrier hopping and intermolecular interactions between conjugated backbones, which thus results in high charge-carrier mobility.[22] In an effort to further extend the linear π-conjugation of the IDT unit, the central phenyl ring was covalently bonded to two thieno[3,2-*b*]thiophenes (TT) to

[a]*Department of Chemical and Biological Engineering/Polymer Technology, Chalmers University of Technology, SE-412 96 Göteborg, Sweden. E-mail: ergang@chalmers.se*
[b]*Ian Wark Research Institute, University of South Australia, Mawson Lakes, Australia. E-mail: mats.andersson@unisa.edu.au*
[c]*Department of Applied Physics, Chalmers University of Technology, SE-412 96 Göteborg, Sweden*

This journal is © The Royal Society of Chemistry 2014

Open Access Article. Published on 30 September 2014. Downloaded on 8/1/2025 7:07:04 PM.
This article is licensed under a Creative Commons Attribution 3.0 Unported Licence.

form the indacenodithieno[3,2-*b*]thiophene (IDTT) arene, which enhances the conjugation of the system through increased planarization on changing the pentacyclic rings to heptacyclic rings. Recently, an IDTT-based polymer with a HOMO level of −5.3 eV and a medium band-gap (E_g) of 1.8 eV was reported by Jen *et al.*, which can attain a PCE of 7%.[23] By copolymerizing IDTT with different acceptor units, tunable optoelectronic properties and charge-carrier mobilities were obtained with PCEs around 4–5%.[24,25] Several architectural designs of devices incorporating non-halogenated solvents and interfacial engineering have resulted in high PCE of 7%.[26,27] However, to expand the family of ladder-type arenes, most efforts have been focused on the designs of building blocks for polymer backbones,[28–33] whilst only a few reports have shed light on the influence of side chain isomerization.[34–36] Recently, we studied two series of thiophene–quinoxaline[37–39] and IDT–quinoxaline[40] copolymers and found that using *meta*-alkyl-phenyl instead of *para*-alkyl-phenyl side chains can enhance the solubility, molecular weight and photovoltaic performances of the copolymers. The corresponding fluorinated IDT-based polymer offered a remarkably high V_{oc} of 0.96 V with a PCE of 6.6%. Meanwhile, the non-fluorinated analogue attained a PCE as high as 7.8%. The planarity and packing distance between the polymer backbones can be varied due to the steric hindrance between adjacent side chains, and then the solubility, molecular weights and packing properties can be changed on a macro level. For the structural optimization of conjugated materials, the proper anchoring of the side groups seems very useful for improving the device efficiency of PSCs. Therefore, here we attempt to extend this side-chain design strategy to the IDTT unit, which so far has been only used in IDT and quinoxaline-based copolymers.

To this end, we have designed and synthesized four copolymers based on the IDTT donor units, and quinoxaline acceptor units (Scheme 2). This is the first direct comparison and evaluation of photovoltaic performances among the IDTT copolymers incorporating different side groups, each of which contains *para*- or *meta*-side chains on pendent phenyl rings. In addition, both non-fluorinated (Q) and fluorinated quinoxaline (QF) acceptor units were chosen for comparison, since the fluorinated acceptor was expected to feature a lower-lying HOMO level due to the electron-withdrawing property of fluorine atoms.[41–47] All polymers were prepared *via* the Stille coupling reaction of bis(trimethylstannyl)-substituted IDTT and dibromo-substituted quinoxaline monomers. The solubility, UV-Vis absorption and electrochemical properties were systematically investigated to understand the structure–property correlations of side chain isomerism and the inclusion of fluorine. BHJ PSCs using $PC_{71}BM$ as the electron acceptor were fabricated for evaluating polymer performance. As anticipated, the devices based on fluorinated copolymers featured higher V_{oc} of close to 1.0 V. Compared to the *para*-substituted analogue PIDTT-Q-*p*, the *meta*-substituted polymer PIDTT-Q-*m*:$PC_{71}BM$ device attains a superior PCE of 6.8%, which is among the highest PCEs of IDTT copolymers recorded for the conversional BHJ PSC configuration. This finding agrees well with our previous study, where polymers with *meta*-substituted side chains show superior photovoltaic performances compared to *para*-substituted analogues. Characterizations of the photoresponse and film morphology indicate that there is a direct correlation between film morphology and device performance for these four copolymers.

Experimental section

Characterization

^{1}H NMR (400 MHz) and ^{13}C NMR (100 MHz) spectra were acquired using a Varian Inova 400 MHz NMR spectrometer. Tetramethylsilane was used as an internal reference with deuterated chloroform as the solvent. Size exclusion chromatography (SEC) was performed on an Agilent PL-GPC 220 Integrated High Temperature GPC/SEC System with refractive index and viscometer detectors. The columns are 3 PLgel 10 μm MIXED-B LS 300 × 7.5 mm columns. The eluent was 1,2,4-trichlorobenzene. The working temperature was 150 °C. The molecular weights were calculated according to relative calibration with polystyrene standards. UV-Vis absorption spectra were measured with a Perkin Elmer Lambda 900 UV-Vis-NIR absorption spectrometer. Square wave voltammetry (SWV) measurements were carried out on a CH-Instruments 650A Electrochemical Workstation. A three-electrode setup was used with platinum wires for both the working electrode and counter electrode, and Ag/Ag^+ was used for the reference electrode calibrated with a ferrocene/ferrocenyl couple (Fc/Fc^+). A 0.1 M nitrogen-saturated solution of tetrabutylammonium hexafluorophosphate (Bu_4NPF_6) in anhydrous acetonitrile was used as the supporting electrolyte. The polymer films were deposited onto the working electrode from chloroform solution. Tapping-mode atomic force microscopy (AFM) images were acquired with an Agilent-5400 scanning probe microscope using a Nanodrive controller with MikroMasch NSC-15 AFM tips and resonant frequencies of ~300 kHz. Transmission electron microscopy (TEM) was performed with a FEI Tecnai T20 (LaB_6, 200 kV). Without LiF/Al electrode deposition, the active layer was placed onto a copper grid using an aqueous dispersion of PEDOT:PSS. The sample was dried at room temperature before the TEM experiments were performed.

Synthesis

All starting materials and reagents were purchased from commercial sources and used without further purification, unless otherwise noted. All reactions involving air-sensitive reagents were performed under a nitrogen atmosphere. Monomer 1 (**M1**),[24] 5,8-bis(5-bromo-thiophen-2-yl)-2,3-bis(3-(octyloxy) phenyl)quinoxaline (**M3**)[11] and 5,8-bis(5-bromothiophen-2-yl)-6,7-difluoro-2,3-bis(3-octyloxyphenyl)quinoxaline (**M4**)[43] were prepared according to literature procedures.

Diethyl 2,5-di(thieno[3,2-*b*]thiophen-2-yl)terephthalate (2)[35]

To a solution of thieno[3,2-*b*]thiophene (2.10 g, 15.0 mmol) in anhydrous THF (30 mL) at −30 °C was added *n*-BuLi (6.3 mL, 2.5 M in hexane), the mixture was kept at −30 °C for 0.5 h and warmed to 0 °C. Then a solution of anhydrous $ZnCl_2$ (2.25 g,

Open Access Article. Published on 30 September 2014. Downloaded on 8/1/2025 7:07:04 PM.
This article is licensed under a Creative Commons Attribution 3.0 Unported Licence.

16.5 mmol) in THF (10 mL) was added slowly. After the addition, the mixture was stirred at 0 °C for 0.5 h. Finally, diethyl 2,5-dibromoterephthalate (**1**) (2.38 g, 6.25 mmol) and $Pd(PPh_3)_4$ (0.14 g, 0.12 mmol) were added to the mixture. The reaction mixture was refluxed for 24 h. After cooling to room temperature, the excess solvent was distilled and the resulting solid was washed successively with ethanol. The residue was collected and purified by column chromatography with 1 : 2 (v/v) ethyl acetate–hexane as the eluent to give the final compound as a yellow solid (2.19 g, 70.2%). ^{1}H NMR (400 MHz, $CDCl_3$), δ (ppm): 7.89 (s, 2H), 7.40 (d, $J = 7.2$ Hz, 2H), 7.30–7.26 (m, 4H), 4.24 (m, 4H), 1.13 (t, $J = 7.2$ Hz, 6H). ^{13}C NMR (100 MHz, $CDCl_3$), δ (ppm): 167.5, 142.0, 139.9, 139.4, 134.1, 133.8, 132.1, 127.4, 119.4, 61.8, 13.8.

Compound 3

To a solution of compound **2** (1.50 g, 3.0 mmol) in anhydrous THF (50 mL) was added a solution of freshly prepared 3-hexylphenyl magnesium bromide from 1-bromo-3-hexylbenzene (3.62 g, 15.0 mmol) in anhydrous THF (30 mL). The solution was refluxed for 12 h. After cooling to room temperature, the organic layer was extracted with ethyl acetate (100 mL), washed successively with saturated brine and then dried over anhydrous $MgSO_4$. The residue was purified by column chromatography with 1 : 15 (v/v) ethyl acetate–hexane as the eluent to afford a crude product as a dark red solid (2.04 g, 64.4%).

Compound 4

Compound **3** (2.0 g, 1.9 mmol) was dissolved in warm glacial acetic acid (100 mL) and conc. H_2SO_4 (2 mL) was added slowly. The reaction mixture was refluxed for 30 min. After cooling to room temperature, the organic layer was extracted with dichloromethane (50 mL), washed successively with 1 M K_2CO_3 aqueous solution and then dried over anhydrous $MgSO_4$. The residue was purified by column chromatography with 1 : 5 (v/v) dichloromethane–hexane as the eluent to give the final compound as a light yellow solid (1.78 g, 92.2%). ^{1}H NMR (400 MHz, $CDCl_3$), δ (ppm): 7.49 (s, 2H), 7.27 (m, 4H), 7.15 (m, 8H), 7.06 (d, $J = 8.0$ Hz, 4H), 7.01 (d, $J = 4.0$ Hz, 4H), 2.52 (t, $J = 8.0$ Hz, 8H), 1.52 (br, 8H), 1.24 (s, 24H), 0.84 (t, $J = 8.0$ Hz, 12H). ^{13}C NMR (100 MHz, $CDCl_3$), δ (ppm): 153.0, 145.8, 143.3, 143.1, 143.0, 141.6, 136.2, 133.7, 128.7, 128.3, 127.2, 126.3, 125.2, 120.3, 116.9, 63.5, 36.0, 31.7, 31.4, 29.0, 22.6, 14.1.

Monomer 2 (M2)

To a solution of compound **4** (1.02 g, 1.0 mmol) in anhydrous THF (10 mL) was added *n*-BuLi (1.0 mL, 2.5 M in hexane) at −30 °C. The reaction mixture was stirred at −30 °C for 0.5 h and then warmed to room temperature for another 2 h. After that, it was cooled to −30 °C again and Me_3SnCl (3.0 mL, 1 M in hexane) was added in one portion. The reaction mixture was stirred at room temperature overnight and then poured into water. The organic layer was extracted with diethyl ether (50 mL), washed successively with water, and dried over anhydrous $MgSO_4$. After removing the solvent, the solid was washed with ethanol. The precipitate was collected as a yellow solid (1.25 g, 93.0%). ^{1}H NMR (400 MHz, $CDCl_3$), δ (ppm): 7.47 (s, 2H), 7.30 (m, 2H), 7.15 (m, 8H), 7.06 (d, $J = 8.0$ Hz, 4H), 7.02 (d, $J = 8.0$ Hz, 4H), 2.54 (t, $J = 8.0$ Hz, 8H), 1.54 (br, 8H), 1.26 (m, 24H), 0.86 (t, $J = 6.0$ Hz, 12H). 0.36 (s, 18H) ^{13}C NMR (100 MHz, $CDCl_3$), δ (ppm): 152.9, 145.3, 143.7, 143.2, 143.0, 140.3, 139.3, 136.4, 128.9, 128.2, 127.3, 127.1, 125.1, 116.8, 63.5, 36.1, 31.8, 31.5, 29.0, 22.6, 14.1, −8.2.

General procedure for polymerization

0.15 mmol of dibromo-substituted monomer, 0.15 mmol of bis(trimethylstannyl)-substituted monomer, tris(dibenzylideneacetone)dipalladium(0) ($Pd_2(dba)_3$) (2.75 mg) and tri(*o*-tolyl) phosphine ($P(o\text{-}Tol)_3$) (3.65 mg) were dissolved in anhydrous toluene (12 mL) under a nitrogen atmosphere. The reaction mixture was refluxed with vigorous stirring for 24 h. After cooling to room temperature, the polymer was precipitated by pouring the solution into acetone and was collected by filtration through a 0.45 μm Teflon filter. Then the polymer was washed in a Soxhlet extractor with acetone, diethyl ether and chloroform. The chloroform fraction was purified by passing it though a short silica gel column and then precipitated from acetone again. Finally, the polymer was obtained by filtration through 0.45 μm Teflon filter and dried under vacuum at 40 °C overnight.

Polymer PIDTT-Q-*p*. 143 mg. Yield: 60%. Molecular weight: $M_n = 33.2$ kDa; $M_w/M_n = 2.9$.

Polymer PIDTT-Q-*m*. 172 mg. Yield: 74%. Molecular weight: $M_n = 41.8$ kDa; $M_w/M_n = 3.2$.

Polymer PIDTT-QF-*p*. 130 mg. Yield: 54%. Molecular weight: $M_n = 14.1$ kDa; $M_w/M_n = 2.2$.

Polymer PIDTT-QF-*m*. 158 mg. Yield: 68%. Molecular weight: $M_n = 17.2$ kDa; $M_w/M_n = 2.2$.

PSC fabrication and characterization

The structure of polymer solar cells was Glass/ITO/PEDOT:PSS/polymer:$PC_{71}BM$/LiF/Al. As a buffer layer, PEDOT:PSS (Baytron P VP Al 4083) was spin-coated onto ITO-coated glass substrates, followed by annealing at 150 °C for 15 minutes to remove water. The thickness of the PEDOT:PSS layer was around 40 nm, as determined by a Dektak 6 M surface profilometer. The active layer consisting of polymers and $PC_{71}BM$ was spin-coated from *o*-dichlorobenzene (*o*DCB) solution onto the PEDOT:PSS layer. The spin-coating was done in a glove box and they were directly transferred to a vapor deposition system mounted inside of the glove box. The thicknesses of active layers were in the range of 85–95 nm. LiF (0.6 nm) and Al (100 nm) were used as the top electrodes and were deposited *via* a mask under vacuum onto the active layer. The accurate area of every device (4.5 mm^2), defined by the overlap of the ITO and metal electrode, was measured carefully by microscope. The PCEs were calculated from the *J–V* characteristics recorded by a Keithley 2400 source meter under the illumination of an AM 1.5G solar simulator with an intensity of 100 mW cm^{-2} (Model SS-50A, Photo Emission Tech., Inc.). The light intensity was determined using a standard silicon photodiode. EQEs were calculated from the photocurrents under short-circuit conditions. The currents

 This journal is © The Royal Society of Chemistry 2014

Open Access Article. Published on 30 September 2014. Downloaded on 8/1/2025 7:07:04 PM.
This article is licensed under a Creative Commons Attribution 3.0 Unported Licence.

were recorded using a Keithley 485 picoammeter under monochromatic light (MS257) illumination through the ITO side of the devices.

Results and discussion

Synthesis of monomers and polymers

The synthetic routes for the monomers are shown in Scheme 1. Diethyl 2,5-di(thieno[3,2-*b*]thiophen-2-yl)terephthalate (**2**) was synthesized by Pd-catalyzed Negishi coupling of diethyl 2,5-dibromoterephthalate (**1**) and thieno[3,2-*b*]thiophen-2-yl zinc chloride, which was freshly prepared from the thieno[3,2-*b*]thiophen-2-yl lithium reagent with anhydrous $ZnCl_2$. In the presence of excess amounts of 3-hexylphenyl magnesium bromide prepared in advanced from 1-bromo-3-hexylbenzene, compound **2** can be transformed to compound **3** in 64% yield. Acid-mediated intramolecular ring closure can afford compound **4** in 92% yield. After lithiation of compound **4** followed by quenching with trimethyltin chloride, the corresponding bis-stannylated monomer **M2** was obtained in a satisfying yield of 93%. The chemical structures of all the compounds were confirmed using ^{1}H NMR and ^{13}C NMR (see the Experimental section for details).

Scheme 2 shows the synthetic routes for the polymers. The polymerizations were accomplished *via* $Pd_2(dba)_3$-catalyzed Stille coupling of the corresponding bis(trimethylstannyl)-substituted monomers **M1**, **M2** and dibromo-substituted monomers **M3**, **M4**, respectively. The same reaction time (24 h) was used for each polymer to study the influences of the side chains and fluorination. After polymerization, the crude polymer was washed in a Soxhlet extractor with acetone and diethyl ether for 24 h each. After that, the polymer was Soxhlet-extracted with chloroform. In this study, the properties of the polymer batches with the highest molecular weights were evaluated providing that they were readily soluble in chloroform, chlorobenzene, and *o*DCB. The molecular weights of the four polymers were measured by size exclusion chromatography (SEC) at 150 °C with 1,2,4-trichlorobenzene as the eluent. The number-average molecular weights (M_n) of the *meta*-substituted polymer PIDTT-Q-*m* and PIDTT-QF-*m* are 41.8 and 17.2 kg mol^{-1} with polydispersity indexes (PDI) of 3.2 and 2.2, respectively. The *para*-substituted polymer PIDTT-Q-*p* and PIDTT-QF-*p* exhibit obviously lower M_n of 33.2 and 14.1 kg mol^{-1}, with PDI of 2.9 and 2.2, respectively. The *meta*-substituted phenyl groups improve the solubility of the IDTT copolymers to provide higher molecular weight copolymers, which thus agree well with our previous study on IDT copolymers.[40] Similar results were also observed in thiophene–quinoxaline (TQ-*m*) copolymers. The kinked *meta*-side chains on quinoxaline moiety result in more twisted polymer backbone, which prevents aggregation in solution and decreases the enthalpy change ΔH_{diss} during dissolution. From the equation: $\Delta G = \Delta H - T\Delta S$ and $T_{diss} = \Delta H_{diss}/\Delta S_{diss}$, the dissolution temperature T_{diss} is reached if the Gibbs free energy $\Delta G = 0$, Therefore, the lower ΔH_{diss} would decrease T_{diss} and improve the solubility of TQ-*m* polymers.[39] Compared to the non-fluorinated analogues, both of the fluorinated IDTT copolymers exhibit lower molecular weights, possibly owing to less coupling activity from increased steric hindrance between the IDTT and fluorinated quinoxaline units.

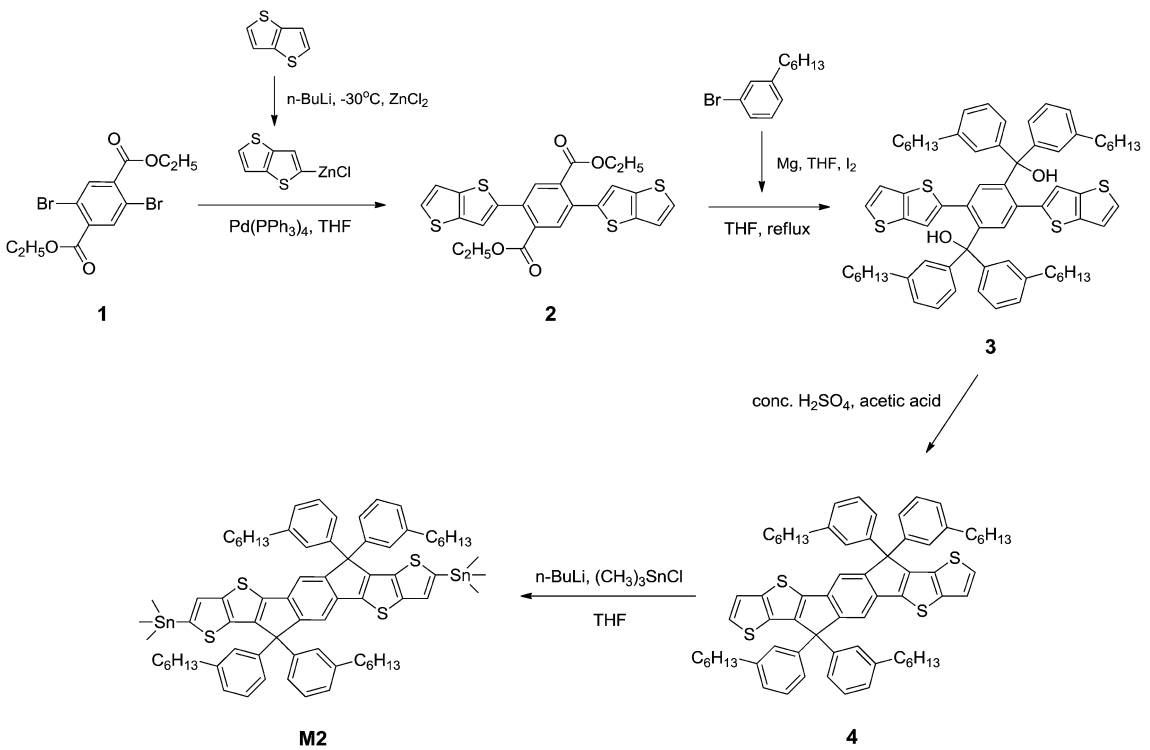

Scheme 1 Synthetic routes of the monomers.

Open Access Article. Published on 30 September 2014. Downloaded on 8/1/2025 7:07:04 PM.
This article is licensed under a Creative Commons Attribution 3.0 Unported Licence.

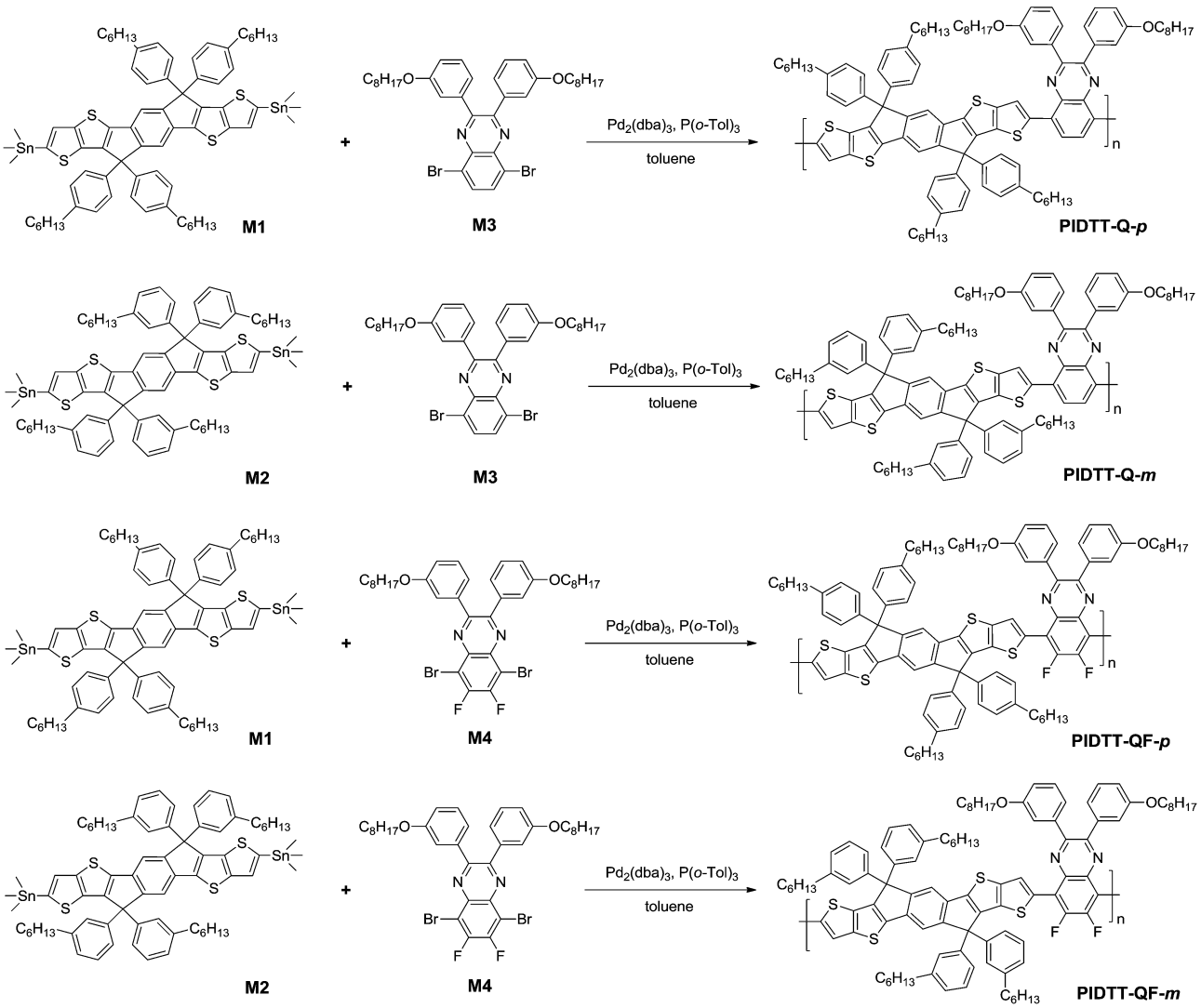

Scheme 2 Synthetic routes and chemical structures of the polymers.

Absorption spectra

The normalized UV-Vis absorption spectra of the four polymers both in chloroform solution and in thin film are shown in Fig. 1. All the polymers depict two distinct absorption bands in the wavelength range of 350–450 and 500–700 nm, corresponding to the π–π* transition and intramolecular charge transfer (ICT) between the IDTT and quinoxaline moieties, respectively. Compared to IDT-based polymers, horizontal extension of π-conjugation by fastening outer TT units efficiently improve the ICT process, since the four IDTT-based polymers here exhibit stronger absorption in the long-wavelength regime.[19] The absorption maxima (λ_{max}) of the polymers PIDTT-Q-*p*, PIDTT-Q-*m*, PIDTT-QF-*p* and PIDTT-QF-*m* in dilute chloroform solutions are around 620 nm (Table 1). A well-resolved shoulder peak is recorded for each of the fluorinated polymers. In thin films, the absorption of the *meta*-substituted polymers PIDTT-Q-*m* and PIDTT-QF-*m* show bathochromic shifts to 630 nm and 643 nm, respectively. A somewhat boarder absorption of the non-fluorinated polymer PIDTT-Q-*m* is observed in comparison to the fluorinated polymer PIDTT-QF-*p*. On the contrary, the *para*-substituted polymers PIDTT-Q-*p* and PIDTT-QF-*p* exhibit little broader spectra in the solid state, λ_{max} values of which shift to 623 nm and 628 nm, respectively. The thin film absorption spectra of the *para*-substituted polymers are comparable this time. These phenomena are related to the different aggregation and π–π stacking characteristics of the polymer backbones caused by the side chain and fluorination. Similar absorption behaviors were also observed in our previous comparison between *meta*- and *para*-substituted IDT polymers.[40] The absorption edges of the film spectra are located around 700 nm. Therefore, the optical band gaps extracted from absorption band edges are similar at around 1.78 eV (Table 1).

Electrochemical properties

The energy levels and band gaps of polymers are the key determinants of their photovoltaic performance, which can be estimated from their corresponding redox curves from electrochemical measurements. As shown in Fig. 2, square-wave

 This journal is © The Royal Society of Chemistry 2014

Open Access Article. Published on 30 September 2014. Downloaded on 8/1/2025 7:07:04 PM.
This article is licensed under a Creative Commons Attribution 3.0 Unported Licence.

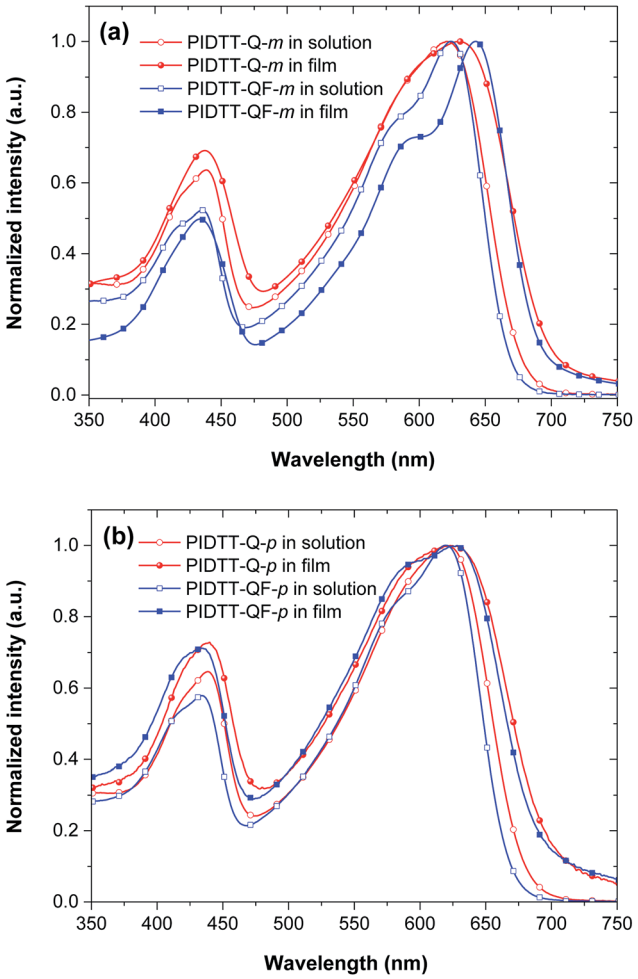

Fig. 1 Normalized UV-Vis absorption spectra of the polymers (a) *meta*-substituted polymer PIDTT-Q-*m* and PIDTT-QF-*m*; (b) *para*-substituted polymer PIDTT-Q-*p* and PIDTT-QF-*p*.

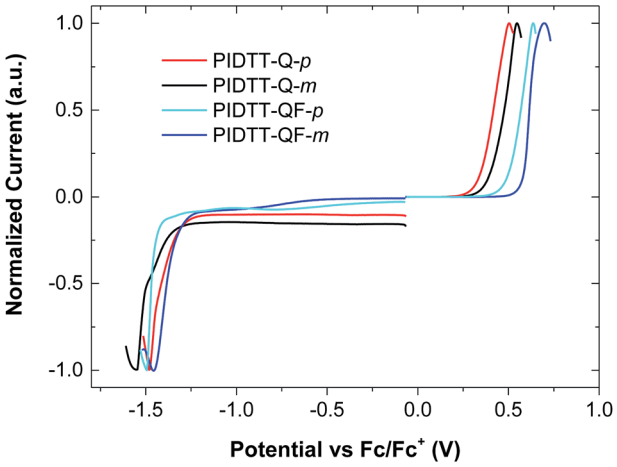

Fig. 2 Square Wave Voltammetries (SWV) of four polymers.

voltammetry (SWV) was used to determine the oxidation (φ_{ox}) and reduction (φ_{red}) potentials of the four polymers. HOMO and LUMO levels were estimated from the peak potentials by setting the oxidative peak potential of Fc/Fc^+ *vs.* the normal hydrogen electrode (NHE) to 0.63 V,[48] and the NHE *vs.* the vacuum level to 4.5 V.[49] HOMO and LUMO levels were calculated according to the formula HOMO $= -(E_{ox} + 5.13)$ eV and LUMO $= -(E_{red} + 5.13)$ eV, where E_{ox} and E_{red} were determined from the oxidation and reduction peaks, respectively.[50] In comparison with the HOMO levels of IDT-based copolymers, those of IDTT-based copolymers are slightly higher in HOMO level due to the more electron-donating TT units on the backbone. The HOMO levels of polymers PIDTT-Q-*p* and PIDTT-Q-*m* are −5.64 eV and −5.68 eV, respectively. As expected, the two fluorinated polymers PIDTT-QF-*p* and PIDTT-QF-*m* display low-lying HOMO levels of −5.76 eV and −5.82 eV, respectively, owing to the electron-withdrawing effect of the fluorine atoms.[40,42,47] Compared to the corresponding *para*-substituted counterparts, the *meta*-substituted polymers PIDTT-Q-*m* and PIDTT-QF-*m* feature a little deeper HOMO levels, which can be attributed to the weaker electron-donating effect from the *meta*-alkyl-phenyl rings.[51] Since the V_{oc} of BHJ PSCs is positively correlated to the energy difference between the HOMO level of electron donor and the LUMO level of electron acceptor, a low-lying HOMO level is a prerequisite for achieving a high V_{oc}. The LUMO levels of the four polymers are −3.65 eV, −3.58 eV, −3.63 eV and −3.67 eV, respectively. The energy difference between the LUMO levels of the four polymers and that of $PC_{71}BM$ (−4.3 eV) are large enough for efficient exciton dissociation. According to the equation, $E_g^{ec} = e(E_{ox} - E_{red})$ (eV), the electrochemical band

Table 1 Optical and electrochemical properties of the polymer

	UV-vis absorption spectra				SWV	
	Solution	Film			p-doping	n-doping
Polymer	λ_{abs} [a] (nm)	λ_{abs} [b] (nm)	λ_{onset} (nm)	E_g^{optc} (eV)	HOMO (eV)	LUMO (eV)
PIDTT-Q-*p*	619	623	703	1.76	−5.64	−3.65
PIDTT-Q-*m*	621	630	702	1.77	−5.68	−3.58
PIDTT-QF-*p*	619	628	694	1.79	−5.76	−3.63
PIDTT-QF-*m*	624	643	691	1.79	−5.82	−3.67

[a] Absorption peak in chloroform solution. [b] Absorption peak in film. [c] Optical band gap.

Open Access Article. Published on 30 September 2014. Downloaded on 8/1/2025 7:07:04 PM.
This article is licensed under a Creative Commons Attribution 3.0 Unported Licence.

gaps of the four polymers are around 2.0 eV. The fluorinated polymers PIDTT-QF-*p* and PIDTT-QF-*m* exhibit slightly boarder band gaps, possibly due to the fact that they are less planar and lower molecular weights.

Photovoltaic properties

To investigate the photovoltaic properties of the four polymers, bulk-heterojunction polymer solar cells (BHJ PSCs) with a device configuration of ITO/PEDOT:PSS/polymer:$PC_{71}BM$/LiF/Al were fabricated. Phenyl-C_{71}-butyric acid methyl ester ($PC_{71}BM$) was used as the electron acceptor due to its good absorption properties across the visible spectrum.[52,53] The measurements of photovoltaic performances were carried out under an illumination of AM 1.5G simulated solar light at 100 mW cm^{-2}. The optimized results were obtained by varying polymer:$PC_{71}BM$ weight ratios, active layer thicknesses, post-annealing conditions and additives. The corresponding PSC parameters (short-circuit current density J_{sc}, open circuit voltage V_{oc}, and fill factor FF) are summarized in Table 2. The *J*–*V* curves are shown in Fig. 3(a), for PIDTT-Q-*m*:$PC_{71}BM$ and PIDTT-Q-*p*:$PC_{71}BM$ based devices, with the corresponding V_{oc} being 0.81 V and 0.83 V, respectively. As anticipated, both devices based on fluorinated copolymers feature a higher V_{oc} of 0.95 V and 0.92 V, respectively, which agrees with their deeper HOMO levels. The *meta*-substituted fluorinated polymer PIDTT-QF-*m* exhibits a slightly higher V_{oc} compared to the *para*-substituted analogue PIDTT-QF-*p*, which is also observed in our previous study of IDT based copolymers. On the other hand, the non-fluorinated polymer PIDTT-Q-*p* and PIDTT-Q-*m* based devices display inverse results with regards to their corresponding V_{oc}. In this case, one possible reason may come from the minor Fermi level shift as a result of the formation of polymer and PCBM aggregates, which can be affected by the domain sizes of D–A components.[54] Without any post-treatment, the PSC using the *meta*-substituted polymer PIDTT-Q-*m* display a superior J_{sc} of 11.8 mA cm^{-2} in comparison with other three copolymers, which results in a PCE of 6.7%. Since these four copolymers show comparable absorption spectra in thin films, the enhanced J_{sc} of the PIDTT-Q-*m* based devices could be ascribed to its higher molecular weight and more favorable nanostructure of its D–A components according to subsequent morphology study. Using 2.5% of DIO as an additives, a slightly higher PCE of 6.8% is recorded, which is one of only a few high-performance results among IDTT based copolymers. This result demonstrates that our side chain isomerization strategy for enhanced photovoltaic performance can be extended from previously studied IDT copolymers to IDTT copolymers.

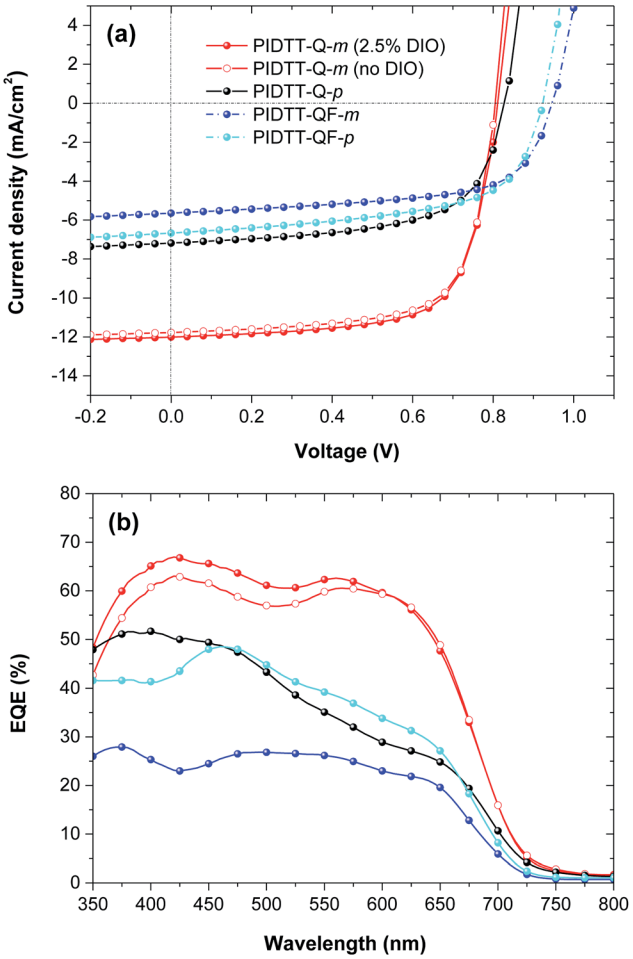

Fig. 3 (a) Current density–voltage characteristics of IDTT copolymer:$PC_{71}BM$ solar cells; (b) external quantum efficiency (EQE) spectra measured under illumination of monochromatic light.

As shown in Fig. 3(b), external quantum efficiencies (EQE) were measured to evaluate the photoresponse of the PSCs. The enhanced quantum efficiency in the region of 400–500 nm is attributable to the absorption of $PC_{71}BM$ in the visible region.[52] The photocurrents calculated *via* integrating the EQE with an AM 1.5G reference spectrum are listed in Table 2, which agrees

Table 2 Photovoltaic parameters of the optimized PSCs

Polymer	Ratio[a]	d^b (nm)	V_{oc} (V)	J_{sc} (mA cm^{-2})	FF	PCE (%)
PIDTT-Q-*p*	1 : 4	90	0.83	7.2 (7.3)[c]	0.63	3.7
PIDTT-Q-*m*	1 : 4	90	0.81	11.8 (11.1)	0.70	6.7
PIDTT-Q-*m* 2.5% DIO[d]	1 : 4	95	0.81	12.0 (11.5)	0.70	6.8
PIDTT-QF-*p*	1 : 4	85	0.92	6.7 (6.8)	0.60	3.7
PIDTT-QF-*m*	1 : 4	90	0.95	5.7 (5.0)	0.63	3.3

[a] Polymer:$PC_{71}BM$ weight ratio. [b] Active layer thickness (*d*). [c] The photocurrents obtained by integrating the EQE spectra (in bracket). [d] 1,8-Diiodooctane.

This journal is © The Royal Society of Chemistry 2014

Open Access Article. Published on 30 September 2014. Downloaded on 8/1/2025 7:07:04 PM.
This article is licensed under a Creative Commons Attribution 3.0 Unported Licence.

well with the corresponding J_{sc} obtained from the *J–V* measurements. Among the four copolymers, the devices based on PIDTT-Q-*m* show higher photo conversion efficiencies over the whole visible region, implying more efficient charge collection and less charge recombination at the junction between the polymer PIDTT-Q-*m* and $PC_{71}BM$. In addition, the corresponding PIDTT-Q-*m* device with 2.5% DIO demonstrates a slightly higher EQE, which is consistent with the *J–V* results.

Film morphology

To further understand the reasons for different photovoltaic performances of the four polymers, the morphology of the active layers were studied by atomic force microscopy (AFM) and transmission electron microscopy (TEM). AFM measurements were carried out to study the surface morphology of the blend layers. As shown in Fig. 4 (AFM), AFM images of the fluorinated copolymers reveal very large polymer domains with a root mean square (RMS) roughness value of 6.9 nm for PIDTT-QF-*p*:$PC_{71}BM$ and 10.1 nm for PIDTT-QF-*m*:$PC_{71}BM$, respectively. Although the domain size of the non-fluorinated PIDTT-Q-*p*:$PC_{71}BM$ blend layer decreases, it also shows a rough surface with RMS roughness of 3.8 nm. For these three copolymers, we propose that the poor miscibility of the D–A components results in a non-optimal nanostructure, which in turn limits the photocurrent of the corresponding devices. The *meta*-substituted non-fluorinated polymer PIDTT-Q-*m*:$PC_{71}BM$ blend layer however forms a continuous, fine phase-segregated morphology of its D–A components with a RMS roughness of 1.2 nm, which depicts a uniform and smooth surface. After mixing 2.5% DIO in the blend, the RMS roughness slightly increases to 1.9 nm, since the additive enables the development of short fibril nanostructures with favorable grain boundaries.[55]

To probe the morphology throughout the active layers, TEM was employed to investigate the real-space images in the polymer-fullerene blends. As shown in Fig. 4 (TEM), the PIDTT-Q-*p*/$PC_{71}BM$ blend layer show large polymer fabric. Both of the PIDTT-QF-*p*/$PC_{71}BM$ and PIDTT-QF-*m*/$PC_{71}BM$ blend layers depict large phase separation, wherein 50–200 nm dark clusters are formed. Since $PC_{71}BM$ has a higher scattering density than the polymer, these dark clusters are ascribed to the aggregation of $PC_{71}BM$.[56] For these three polymers, the dimensions of the phase separation and the discontinuous networks are much larger than the typical exciton diffusion length (10 nm), and thus the photogenerated excitons may recombine more easily during exciton diffusion. This may result in poor exciton separation, a low J_{sc} and thereby limit the corresponding device performance. The PIDTT-QF-*m*/$PC_{71}BM$ blend layer has even bigger domain size compared to the PIDTT-QF-*p*/$PC_{71}BM$ blend, which is consistent with its lower PCE than the PIDTT-QF-*p* based device. On the contrary, a significant reduction of the phase separation is observed in the PIDTT-Q-*m*:$PC_{71}BM$ blends. Both of the blend films with and without DIO form continuous and tiny $PC_{71}BM$ aggregates. On the basis of the observations from AFM and TEM images, it is evident that the polymer PIDTT-Q-*m*/$PC_{71}BM$ has the most favorable morphology among these four blend layers. Continuous pathways have been formed properly, which subsequently enhance exciton diffusion as well as charge separation. As a result, more efficient exciton diffusion and dissociation in D–A phases correlate well with the superior J_{sc} and PCE obtained for the PIDTT-Q-*m* based devices. Similar morphological properties were observed in our previous study of *meta*-substituted IDT-based copolymers. The different molecular conformation and solid state order of the IDTT copolymers may affect the film morphology. From the previous density functional theory (DFT) calculations of the IDT copolymers, the *meta*-substituted side chains tend to wrap around the conjugated backbone, while the *para*-substituted side chains extend from the conjugated backbone in all directions. This extended side-chain conformation raises steric hindrance between adjacent chains, and thus a larger distance between polymer backbones were recorded *via* the grazing-incidence wide-angle X-ray scattering (GIWAXS).[40]

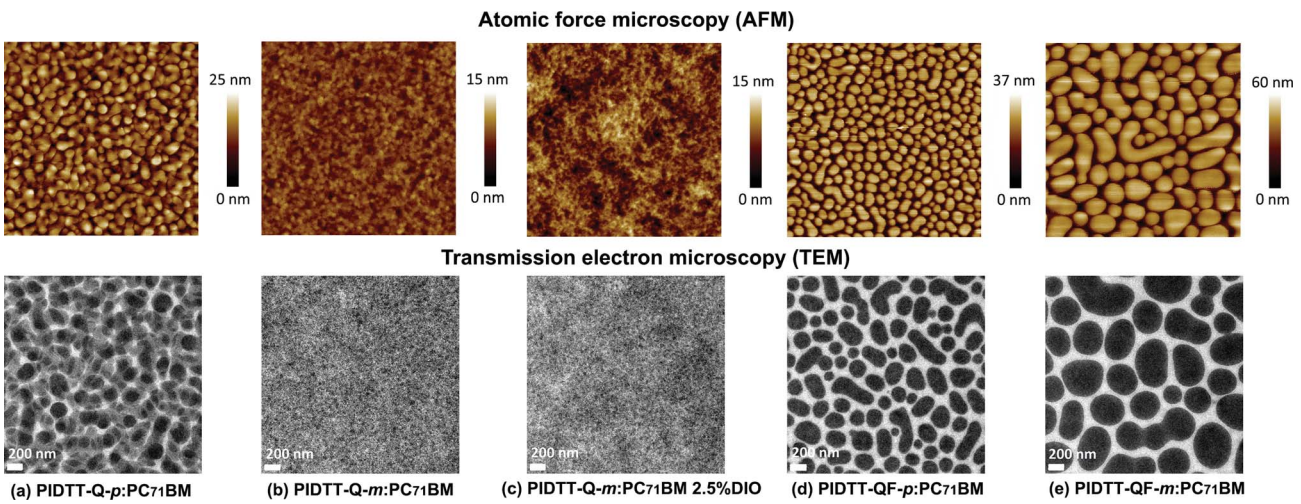

Fig. 4 AFM topography (5 × 5 μm^2) and TEM bright field images of optimized IDTT copolymer:$PC_{71}BM$ blended layers.

Open Access Article. Published on 30 September 2014. Downloaded on 8/1/2025 7:07:04 PM.
This article is licensed under a Creative Commons Attribution 3.0 Unported Licence.

Conclusion

In summary, two pairs of IDTT-quinoxaline based copolymers with *para*-hexyl-phenyl or *meta*-hexyl-phenyl side chains on the IDTT units were synthesized and characterized to understand the effect of side chain isomerization. As anticipated, the BHJ PSCs based on the fluorinated polymers PIDTT-QF-*p* and PIDTT-QF-*m* offer a high V_{oc} of 0.92 V and 0.95 V, respectively. The *meta*-substituted polymers PIDTT-Q-*m* and PIDTT-QF-*m* offer better solubility and higher molecular weights. Although positioning the alkyl side chain in either the *para*- or *meta*-position of the phenyl ring has little influence on the absorption and energy levels as well as the band gaps of corresponding copolymers, it plays an important role in forming a more appropriate and fine-grained nanostructure in the D–A blend. As a result, the PIDTT-Q-*m*:$PC_{71}BM$ device attains a superior photocurrent and a PCE as high as 6.8%. This result is among the highest efficiency achieved for IDTT copolymers used in conversional BHJ PSCs. It is also a comparatively high value for board band-gap polymers, with band gaps around 1.8 eV, which enables the PIDTT-Q-*m* polymer to be an appealing candidate for the front cell of tandem devices. Gratifyingly, we demonstrate that the *meta*-alkyl-phenyl substituted IDTT moiety is a promising building block for efficient organic photovoltaic materials. In our forthcoming work, through further structural optimization of the electron-withdrawing moieties and pendent side groups, it is entirely feasible to synthesize higher-performing IDTT-based conjugated molecules and polymers. Moreover, the here discussed structure–property correlations attest and extend our side-chain design strategy to IDTT-based copolymers, which is expected to be quite valuable for enhancing the photovoltaic performance of conjugated polymers.

Acknowledgements

We thank the Swedish Research Council, the Swedish Energy Agency and the EU projects SUNFLOWER-"SUstainable Novel FLexible Organic Watts Efficiently Reliable" (FP7-ICT-2011-7, Grant number: 287594) and OSNIRO (FP7-PEOPLE-2013-ITN, Grant agreement no.: 607585) for financial support.

Notes and references

1 C. J. Brabec, N. S. Sariciftci and J. C. Hummelen, *Adv. Funct. Mater.*, 2001, **11**, 15.
2 B. C. Thompson and J. M. J. Fréchet, *Angew. Chem., Int. Ed.*, 2008, **47**, 58.
3 F. C. Krebs, S. A. Gevorgyan and J. Alstrup, *J. Mater. Chem.*, 2009, **19**, 5442.
4 A. J. Heeger, *Adv. Mater.*, 2014, **26**, 10.
5 Z. He, C. Zhong, S. Su, M. Xu, H. Wu and Y. Cao, *Nat. Photonics*, 2012, **6**, 591.
6 Y.-J. Cheng, S.-H. Yang and C.-S. Hsu, *Chem. Rev.*, 2009, **109**, 5868.
7 J. Chen and Y. Cao, *Acc. Chem. Res.*, 2009, **42**, 1709.
8 E. Wang, W. Mammo and M. R. Andersson, *Adv. Mater.*, 2014, **26**, 1801.
9 H. Zhou, L. Yang and W. You, *Macromolecules*, 2012, **45**, 607.
10 J. M. Szarko, J. Guo, Y. Liang, B. Lee, B. S. Rolczynski, J. Strzalka, T. Xu, S. Loser, T. J. Marks, L. Yu and L. X. Chen, *Adv. Mater.*, 2010, **22**, 5468.
11 E. Wang, L. Hou, Z. Wang, Z. Ma, S. Hellström, W. Zhuang, F. Zhang, O. Inganäs and M. R. Andersson, *Macromolecules*, 2011, **44**, 2067.
12 A. T. Yiu, P. M. Beaujuge, O. P. Lee, C. H. Woo, M. F. Toney and J. M. Frechet, *J. Am. Chem. Soc.*, 2012, **134**, 2180.
13 T. Lei, J.-H. Dou and J. Pei, *Adv. Mater.*, 2012, **24**, 6457.
14 I. Meager, R. S. Ashraf, S. Mollinger, B. C. Schroeder, H. Bronstein, D. Beatrup, M. S. Vezie, T. Kirchartz, A. Salleo, J. Nelson and I. McCulloch, *J. Am. Chem. Soc.*, 2013, **135**, 11537.
15 K. Takimiya, S. Shinamura, I. Osaka and E. Miyazaki, *Adv. Mater.*, 2011, **23**, 4347.
16 K.-T. Wong, T.-C. Chao, L.-C. Chi, Y.-Y. Chu, A. Balaiah, S.-F. Chiu, Y.-H. Liu and Y. Wang, *Org. Lett.*, 2006, **8**, 5033.
17 C.-P. Chen, S.-H. Chan, T.-C. Chao, C. Ting and B.-T. Ko, *J. Am. Chem. Soc.*, 2008, **130**, 12828.
18 Y.-C. Chen, C.-Y. Yu, Y.-L. Fan, L.-I. Hung, C.-P. Chen and C. Ting, *Chem. Commun.*, 2010, **46**, 6503.
19 Y. Zhang, J. Zou, H.-L. Yip, K.-S. Chen, D. F. Zeigler, Y. Sun and A. K. Y. Jen, *Chem. Mater.*, 2011, **23**, 2289.
20 M. Wang, X. Hu, L. Liu, C. Duan, P. Liu, L. Ying, F. Huang and Y. Cao, *Macromolecules*, 2013, **46**, 3950.
21 X. Guo, M. Zhang, J. Tan, S. Zhang, L. Huo, W. Hu, Y. Li and J. Hou, *Adv. Mater.*, 2012, **24**, 6536.
22 W. Zhang, J. Smith, S. E. Watkins, R. Gysel, M. McGehee, A. Salleo, J. Kirkpatrick, S. Ashraf, T. Anthopoulos, M. Heeney and I. McCulloch, *J. Am. Chem. Soc.*, 2010, **132**, 11437.
23 Y.-X. Xu, C.-C. Chueh, H.-L. Yip, F.-Z. Ding, Y.-X. Li, C.-Z. Li, X. Li, W.-C. Chen and A. K. Y. Jen, *Adv. Mater.*, 2012, **24**, 6356.
24 H.-H. Chang, C.-E. Tsai, Y.-Y. Lai, D.-Y. Chiou, S.-L. Hsu, C.-S. Hsu and Y.-J. Cheng, *Macromolecules*, 2012, **45**, 9282.
25 Y.-X. Xu, C.-C. Chueh, H.-L. Yip, C.-Y. Chang, P.-W. Liang, J. J. Intemann, W.-C. Chen and A. K. Y. Jen, *Polym. Chem.*, 2013, **4**, 5220.
26 C.-C. Chueh, K. Yao, H.-L. Yip, C.-Y. Chang, Y.-X. Xu, K.-S. Chen, C.-Z. Li, P. Liu, F. Huang, Y. Chen, W.-C. Chen and A. K. Y. Jen, *Energy Environ. Sci.*, 2013, **6**, 3241.
27 J. J. Intemann, K. Yao, Y.-X. Li, H.-L. Yip, Y.-X. Xu, P.-W. Liang, C.-C. Chueh, F.-Z. Ding, X. Yang, X. Li, Y. Chen and A. K. Y. Jen, *Adv. Funct. Mater.*, 2014, **24**, 1465.
28 T. W. Lee, N. S. Kang, J. W. Yu, M. H. Hoang, K. H. Kim, J.-I. Jin and D. H. Choi, *J. Polym. Sci., Part A: Polym. Chem.*, 2010, **48**, 5921.
29 H. Bronstein, R. S. Ashraf, Y. Kim, A. J. P. White, T. Anthopoulos, K. Song, D. James, W. Zhang and I. McCulloch, *Macromol. Rapid Commun.*, 2011, **32**, 1664.
30 J.-S. Wu, Y.-J. Cheng, T.-Y. Lin, C.-Y. Chang, P.-I. Shih and C.-S. Hsu, *Adv. Funct. Mater.*, 2012, **22**, 1711.
31 Y.-L. Chen, C.-Y. Chang, Y.-J. Cheng and C.-S. Hsu, *Chem. Mater.*, 2012, **24**, 3964.

 This journal is © The Royal Society of Chemistry 2014

Open Access Article. Published on 30 September 2014. Downloaded on 8/1/2025 7:07:04 PM.
This article is licensed under a Creative Commons Attribution 3.0 Unported Licence.

32 Y. Ma, Q. Zheng, Z. Yin, D. Cai, S.-C. Chen and C. Tang, *Macromolecules*, 2013, **46**, 4813.
33 J.-S. Wu, Y.-Y. Lai, Y.-J. Cheng, C.-Y. Chang, C.-L. Wang and C.-S. Hsu, *Adv. Energy Mater.*, 2013, **3**, 457.
34 C.-Y. Chang, Y.-J. Cheng, S.-H. Hung, J.-S. Wu, W.-S. Kao, C.-H. Lee and C.-S. Hsu, *Adv. Mater.*, 2012, **24**, 549.
35 X. Xu, P. Cai, Y. Lu, N. S. Choon, J. Chen, B. S. Ong and X. Hu, *Macromol. Rapid Commun.*, 2013, **34**, 681.
36 C.-P. Chen and H.-L. Hsu, *Macromol. Rapid Commun.*, 2013, **34**, 1623.
37 E. Wang, L. Hou, Z. Wang, S. Hellström, F. Zhang, O. Inganäs and M. R. Andersson, *Adv. Mater.*, 2010, **22**, 5240.
38 L. Hou, E. Wang, J. Bergqvist, B. V. Andersson, Z. Wang, C. Müller, M. Campoy-Quiles, M. R. Andersson, F. Zhang and O. Inganäs, *Adv. Funct. Mater.*, 2011, **21**, 3169.
39 E. Wang, J. Bergqvist, K. Vandewal, Z. Ma, L. Hou, A. Lundin, S. Himmelberger, A. Salleo, C. Müller, O. Inganäs, F. Zhang and M. R. Andersson, *Adv. Energy Mater.*, 2013, **3**, 806.
40 D. Dang, W. Chen, S. Himmelberger, Q. Tao, A. Lundin, R. Yang, W. Zhu, A. Salleo, C. Müller and E. Wang, *Adv. Energy Mater.*, 2014, 1400680.
41 Y. Liang, D. Feng, Y. Wu, S.-T. Tsai, G. Li, C. Ray and L. Yu, *J. Am. Chem. Soc.*, 2009, **131**, 7792.
42 H. Zhou, L. Yang, A. C. Stuart, S. C. Price, S. Liu and W. You, *Angew. Chem., Int. Ed.*, 2011, **50**, 2995.
43 D. Dang, W. Chen, R. Yang, W. Zhu, W. Mammo and E. Wang, *Chem. Commun.*, 2013, **49**, 9335.
44 Y. Zhang, S.-C. Chien, K.-S. Chen, H.-L. Yip, Y. Sun, J. A. Davies, F.-C. Chen and A. K. Y. Jen, *Chem. Commun.*, 2011, **47**, 11026.
45 S. Albrecht, S. Janietz, W. Schindler, J. Frisch, J. Kurpiers, J. Kniepert, S. Inal, P. Pingel, K. Fostiropoulos, N. Koch and D. Neher, *J. Am. Chem. Soc.*, 2012, **134**, 14932.
46 J. Min, Z.-G. Zhang, S. Zhang and Y. Li, *Chem. Mater.*, 2012, **24**, 3247.
47 S. C. Price, A. C. Stuart, L. Yang, H. Zhou and W. You, *J. Am. Chem. Soc.*, 2011, **133**, 4625.
48 V. V. Pavlishchuk and A. W. Addison, *Inorg. Chim. Acta*, 2000, **298**, 97.
49 A. J. Bard and L. R. Faulkner, *Electrochemical Methods: Fundamentals and Applications*, Wiley, 2000.
50 S. Hellstrom, F. Zhang, O. Inganas and M. R. Andersson, *Dalton Trans.*, 2009, 10032.
51 Y. Huang, M. Zhang, L. Ye, X. Guo, C. C. Han, Y. Li and J. Hou, *J. Mater. Chem.*, 2012, **22**, 5700.
52 M. M. Wienk, J. M. Kroon, W. J. H. Verhees, J. Knol, J. C. Hummelen, P. A. van Hal and R. A. J. Janssen, *Angew. Chem., Int. Ed.*, 2003, **42**, 3371.
53 Y. He and Y. Li, *Phys. Chem. Chem. Phys.*, 2011, **13**, 1970.
54 D. Veldman, Ö. İpek, S. C. J. Meskers, J. Sweelssen, M. M. Koetse, S. C. Veenstra, J. M. Kroon, S. S. V. Bavel, J. Loos and R. A. J. Janssen, *J. Am. Chem. Soc.*, 2008, **130**, 7721.
55 S. J. Lou, J. M. Szarko, T. Xu, L. Yu, T. J. Marks and L. X. Chen, *J. Am. Chem. Soc.*, 2011, **133**, 20661.
56 C. M. Amb, S. Chen, K. R. Graham, J. Subbiah, C. E. Small, F. So and J. R. Reynolds, *J. Am. Chem. Soc.*, 2011, **133**, 10062.